

## Supporting Information

### **Intermolecular Chemistry in High-Entropy Solid Polymer Electrolyte Enabling Room Temperature Solid-State Lithium Metal Batteries**

Hui-Juan Guo,<sup>a</sup> Rui Shu,<sup>a</sup> Ya-Xin Xie,<sup>a</sup> Xue-Ying Wang,<sup>a</sup> Hao-Nan Wu,<sup>a</sup> Yue-Xian Song,<sup>b</sup> Jian-Xin Tian,<sup>c</sup> Fan-Peng Cheng,<sup>a</sup> Yang-Yang Guo,<sup>\*d</sup> Tingyu Zhu,<sup>d</sup> Li-Juan Shi<sup>\*a</sup> Rui Wen,<sup>c</sup> and Qun Yi<sup>\*a</sup>

<sup>a</sup> Key Laboratory of Green Chemical Process of Ministry of Education, State Key laboratory of Green and efficient Development of Phosphorus Resources, Key Laboratory of Novel Reactor and Green Chemical Technology of Hubei Province, School of Chemical Engineering and Pharmacy, Wuhan Institute of Technology  
Wuhan 430205, China

E-mail: shilijuanwit@sina.com; yq20071001@163.com

<sup>b</sup> School of Energy and Power Engineering, North University of China  
Taiyuan 030051, China

<sup>c</sup> Institute of Process Engineering, Chinese Academy of Sciences, National Engineering Laboratory for Hydrometallurgical Cleaner Production Technology  
Beijing 100190, China

E-mail: yyguo@ipe.ac.cn

<sup>d</sup> CAS Key Laboratory of Molecular Nanostructure and Nanotechnology, CAS Research/Education Center for Excellence in Molecular Sciences, Beijing National Laboratory for Molecular Sciences (BNLMS), Institute of Chemistry, Chinese Academy of Sciences (CAS)  
Beijing 100190, China

## Experiments and Methods

### Material Characterization

X-ray diffraction (XRD) technique (Bruker D8 ADVANCE) was performed in the  $2\theta$  range from  $10^\circ$  to  $80^\circ$  at  $1^\circ \text{ min}^{-1}$  scan rate to examine the crystallinity of electrolytes. Thermogravimetric curves of the samples were obtained through a TGA thermoanalyzer (TA Discovery SDT 650) with a nitrogen atmosphere. Differential scanning calorimeter (DSC, TA Discovery SDT 650), Raman (Thermo Scientific, DXR), Fourier transform infrared spectroscopy (FTIR, Bruker VERTEX 33) and X-ray photoelectron spectroscopy (XPS, Thermo Fisher ESCALAB XI+) were performed to test the phase transition behavior and chemical structure of electrolytes, respectively. The morphologies of electrolytes and lithium metals were observed by scanning electron microscopy (Gemini SEM 300) and an energy-dispersive X-ray spectrometer (EDS) was used to perform elemental surface distribution tests. Samples for  $^1\text{H}$  nuclear magnetic resonance (NMR) were dissolved in  $\text{D}_2\text{O}$  and measured on a Bruker AVANCE NEO. The DMT modulus was determined by AFM (Bruker Corp., Dimension Icon) in a glovebox (Mikrouna, Super 1220/750,  $\text{H}_2\text{O} < 0.1 \text{ ppm}$ ,  $\text{O}_2 < 0.1 \text{ ppm}$ ) filled with high purity argon (Ar).

### Configurational entropy

According to thermodynamics, Gibbs free energy ( $G$ ) is determined by temperature ( $T$ ), entropy ( $S$ ) and enthalpy ( $H$ ) of the system as follows:

$$\Delta G = \Delta H - T\Delta S \quad (1)$$

By introducing multiple components to enhance  $S$ , it becomes possible to mitigate the impact of the increased  $H$  and thereby reduce the Gibbs free energy, thus improving the stability and reaction rate of electrolytes.<sup>[1]</sup>

According to Equation (2), the introduction of multiple components increases the local disorder, resulting in a higher  $S_{\text{config}}$ :

$$S_{\text{config}} = -R \sum_{i=1}^n x_i \ln x_i \quad (2)$$

Where  $R$  denotes the ideal gas constant,  $x_i$  represents the mole fraction of components (ions presented in cation and anion site or the coordination groups of lithium ions), and  $n$  is the number of components.<sup>[2]</sup> It can be seen that the  $S_{\text{config}}$  of the as-prepared HESZ-SPE is estimated as 1.57 R, which belongs to the “high entropy” group ( $>1.5 \text{ R}$ ) and exceeds that of general amorphous disorder PEO-SPE (1.28 R).

The modulus-entropy relationship in SPEs is accurately described by Equation (3).

$$F = -T \frac{dS(L)}{dL} \quad (3)$$

According to Equation (3), if the entropy (S) of the system is higher, the external force (F) would be greater for the same average length (L). Hence, high-entropy structure design significantly enhances the mechanical strength of SPE.

### Electrochemical measurements

All electrochemical tests of solid-state electrolytes were performed by adopting 2032 button battery. The ionic conductivity of solid-state electrolyte was measured via electrochemical impedance spectroscopy (EIS) method with assembled stainless-steel (SS) symmetric battery (SS|electrolyte|SS) over the temperature range from 20 to 80 °C. The tests voltage and frequency range were 0.01 V and 1 HZ-10<sup>6</sup> HZ, respectively. The ionic conductivity can be calculated by Equation (4):

$$\sigma = \frac{L}{R \times S} \quad (4)$$

where L is the thickness of electrolyte, R represents interface resistance of electrolyte, S is the contact area of electrolyte membrane. [3]

The lithium-ion transference number ( $t_{Li^+}$ ) was evaluated via chronoamperometry and electrochemical impedance spectroscopy with assembled lithium symmetric battery (Li|electrolyte|Li) at room temperature. The Li<sup>+</sup>-transference number can be calculated by the Equation (5):

$$t_{Li^+} = \frac{I_{ss}(\Delta V - I_0 \times R_0)}{I_0(\Delta V - I_{ss} \times R_{ss})} \quad (5)$$

where  $\Delta V$ ,  $I_0$ ,  $I_{ss}$ ,  $R_0$ , and  $R_{ss}$  represent the polarization potential (10 mV), the initial current, steady current, initial interfacial resistance, and steady interfacial resistance, respectively.

CV curves of the LFP/Li batteries were recorded in 2.5–4.0 V, and equation (6) is used to calculate the Li<sup>+</sup> diffusion coefficient.

$$I_p = 2.68 \times 10^5 n^{3/2} A D^{1/2} C \omega^{1/2} \quad (6)$$

where A,  $\omega$ , D and C are the cathode area (1.13 cm<sup>2</sup>), the potential scan rate (V s<sup>-1</sup>), the diffusion coefficient (cm<sup>2</sup> s<sup>-1</sup>) and the initial Li<sup>+</sup> concentration in the cathode (7.7767×10<sup>-4</sup> mol cm<sup>-3</sup>), respectively. The n and I<sub>p</sub> are the number of electrons in reaction (n = 1), and the peak current, respectively. [4]

The electrochemical stability window of solid-state electrolyte was determined by linear scanning voltammetry method (LSV) with asymmetric batteries (SS|electrolyte|Li). The tests voltage ranges from 0 to 7 V.

For Li | electrolyte | Li battery, the critical current density (CCD) was tested by the LANHE CT3002 A, with galvanostatic charging and discharging at current densities ranging from 0.1 to 3 mA cm<sup>-2</sup>, increasing by 0.1 mA cm<sup>-2</sup> per cycle.

The rate performance, cycling stability, charge–discharge capacity and coulombic efficiency of solid-state electrolyte was evaluated based on the LANHE CT3002A charge/discharge cycle system at room temperature. The Li plating/stripping cycle ability was investigated via assembled Li|electrolyte|Li symmetric batteries with the current density limit from 0.01 to 0.40 mA cm<sup>-2</sup>. The long-term cycling testing was obtained by galvanostatic charging and discharging at current densities of 0.1 mA cm<sup>-2</sup>.

The rate performance of the solid-state electrolyte was measured by assembled LFP||Li asymmetric battery with the current density from 0.1 to 2.0 C (1.0 C = 170 mA g<sup>-1</sup>) as well as the voltage ranging from 2.5 to 4.0 V.

The cycling ability, charge–discharge capacity and coulomb efficiency were investigated by assembled LiFePO<sub>4</sub>|electrolyte|Li symmetric battery with the current density of 0.2 C (1.0 C = 170 mA g<sup>-1</sup>) and the voltage ranging from 2.5 to 4.0 V. Moreover, rate capability tests were performed up to 0.5 C to demonstrate stability behaviour of SPE under high current rate.

Electrochemical impedance spectroscopy (EIS) testing was carried out using an Autolab electrochemical workstation (Metrohm Autolab, PGSTAT302N) over frequency ranges from 1 to 10<sup>6</sup> Hz with an AC amplitude of 10 mV.

### **Molecular dynamics simulations**

The MD simulation simulations were performed using the Materials Studio 2019 software. First, a periodic simulation box with fixed amounts of PZ, PEO and LiTFSI (PZ : PEO : LiTFSI = 1 : 1 : 29) was created by an amorphous cell. Next, the unit cell was optimized by the energy minimization and MD simulation in the NPT ensemble. The total simulation time was 100 ns, in the NPT ensemble, the time step was 1 fs, and the trajectory was recorded every 20 fs. Electrostatic interaction and van der Waals interaction adopted Ewald summation and Atom-based summation, respectively, with a calculation accuracy of 1×10<sup>-5</sup> kcal mol<sup>-1</sup> and a spline cut off distance of 10 Å. The COMPASS III force field was used for the whole process. The periodic box size was set as 2.6\*2.6\*2.6 nm, with periodic boundary conditions (PBCs) applied in all three directions. Using the V-rescale and Parrinello-Rahman temperature and pressure coupling algorithms, the system was then pre-equilibrated in an NPT ensemble at pressures of 1 atm and 303 K. Finally, the simulation results' mean square displacement (MSD) was analyzed by Forcite module.

### **Density functional theory (DFT) calculations**

Geometry optimization of all the molecules was first performed via Gaussian 16 at the B3LYP/def2tzvp level to obtain rational structures. The vdW interactions were described using DFT-D3(BJ) dispersion correction. Moreover, The Visual Molecular Dynamics (VMD) and Multiwfn software were used for analysis, isovalue = 0.04.<sup>[5]</sup>

$$Eb = EA - B - EA - EB \quad (7)$$

$E_b$  is the total energy of A with coordinated B,  $E_A$  is the single-point energy of A,  $E_B$  is the single-point energy of B.

### Finite Element Simulation

Based on COMSOL Multiphysics 6.2 software, the  $\text{Li}^+$  concentration distribution, anion concentration distribution and electric potential spatial distribution in composite electrolytes were studied by finite element method (FEM).<sup>[6]</sup> The simulation is based on the coupling model of two modules, "dilute material transfer" and "static electricity". The plating/stripping of  $\text{Li}^+$  is described by the Butler Volmer kinetic equation (8).<sup>[7]</sup>

$$i = i_0 \left( \exp\left(\frac{\alpha_a F \eta}{RT}\right) - \exp\left(-\frac{\alpha_c F \eta}{RT}\right) \right) \quad (8)$$

The flux at the electrolyte boundary is coupled to the electrochemical reaction according to Faraday's law. The migration of  $\text{Li}^+$  and anions driven by an electric field is governed by the Nernst-Planck-Poisson equation (9). The Nernst-Planck equation is implemented as follows:

$$J_i = D_i \left( \nabla c_i + \frac{z_i F c_i}{RT} \nabla \varphi \right) + c_i u \quad (9)$$

Where  $J_i$  represents the current density,  $D_i$  denotes the diffusion coefficient,  $\nabla c_i$  signifies the concentration gradient,  $z_i$  stands for the charge density,  $F$  is the Faraday constant (96,485.34 C/mol),  $R$  is the gas constant (8.3145 J/(mol·K)),  $\nabla \varphi$  is the potential difference, and  $u$  represents the velocity. In cases where fluid flow is not considered,  $u = 0$ . According to Nernst-Einstein equation (10),  $D$  can be determined by the ionic conductivity<sup>[8]</sup>.

$$\sigma = D \frac{nq^2}{KT} \quad (10)$$

where  $K$  is the Boltzmann constant,  $q$  is the charge of the charge carriers,  $D$  is the diffusion coefficient, and  $T$  is the temperature. In addition, the law of conservation of mass (11) and the condition of electroneutrality (12) are guaranteed by the following equations:

$$\frac{\partial c_i}{\partial t} = -\nabla N_i, i = 1, 2, \dots \quad (11)$$

$$0 = \sum_i z_i c_i \quad (12)$$

The Poisson equation is implemented as follows:

$$E = -\nabla\varphi \quad (13)$$

where  $\varphi$  is the overpotential, which is considered as the coupling term with Nernst-Planck equation.  $E$  is the electric field. As the driving force for  $\text{Li}^+$  transport, the potential difference between the anode and cathode was set as 0.1 V. All parameters related to the electrolyte are actually measured values and are summarized in Supplementary Tables 3 and 4.

## Results and Discussion

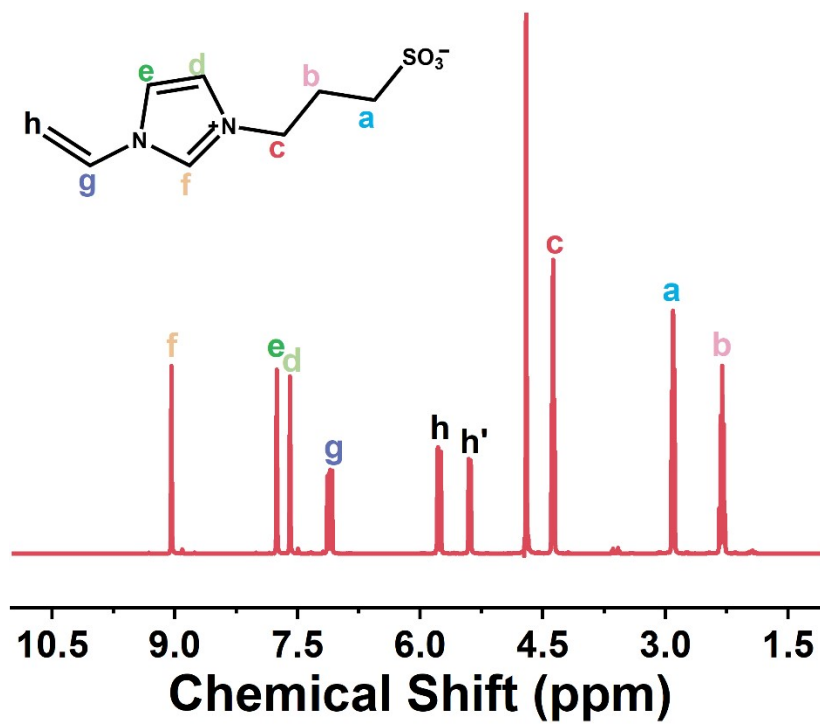
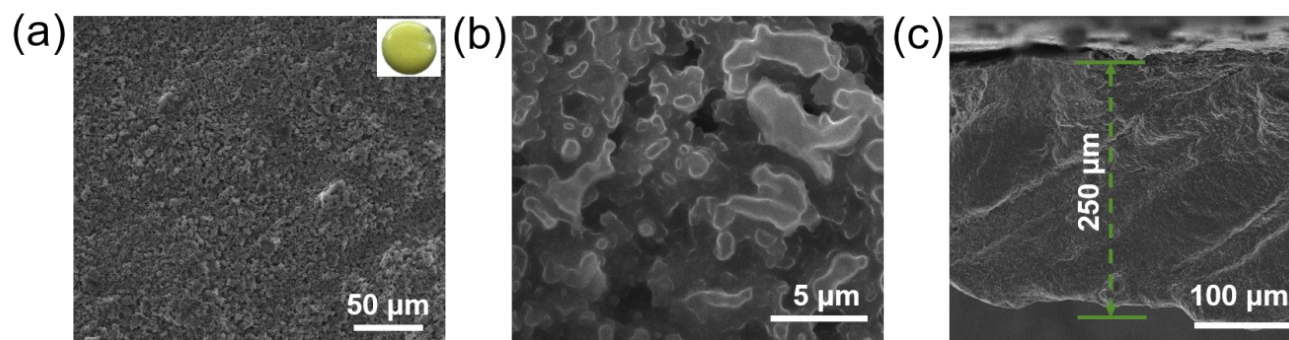
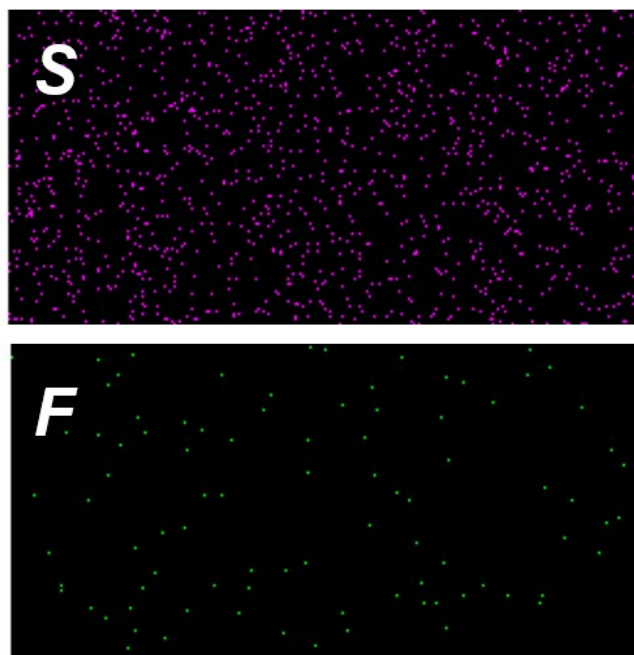


Figure S1. <sup>1</sup>H NMR spectrum (D<sub>2</sub>O) of synthesis of VIPS.



**Figure S2.** SEM images of HESZ-SPE. The scale bar is 50  $\mu\text{m}$  (a), 5  $\mu\text{m}$  (b), and 100  $\mu\text{m}$  (c).



**Figure S3.** EDS maps of designed HESZ-SPE.

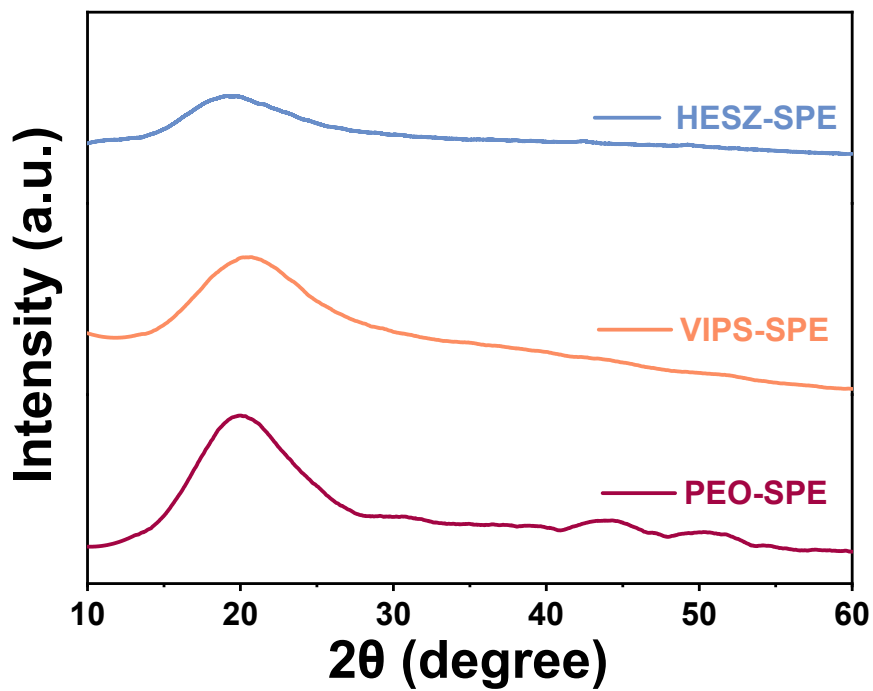


**Figure S4.** XRD patterns of PEO-SPE, VIPS-SPE and HESZ-SPE.

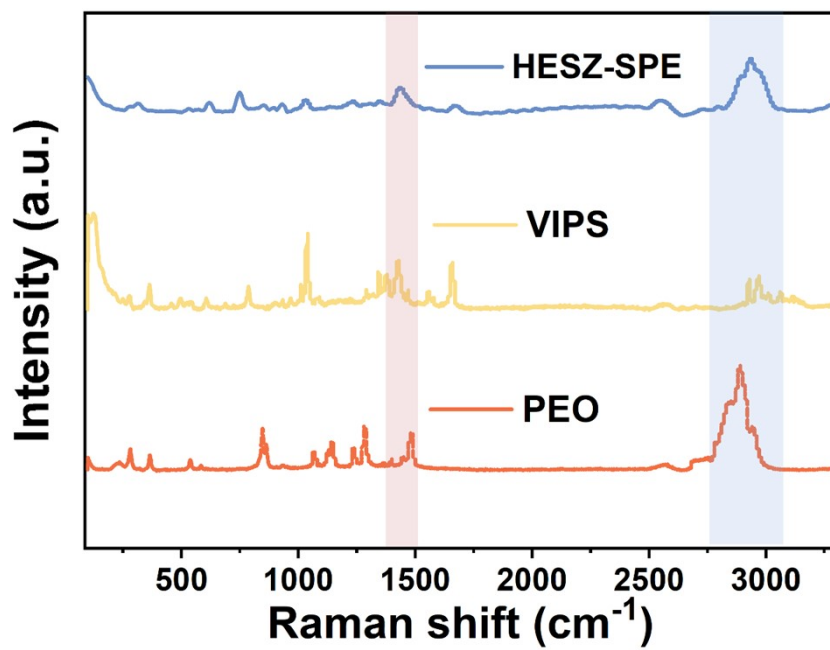


**Figure S5.** Raman spectra of PEO, VIPS and designed HESZ-SPE.

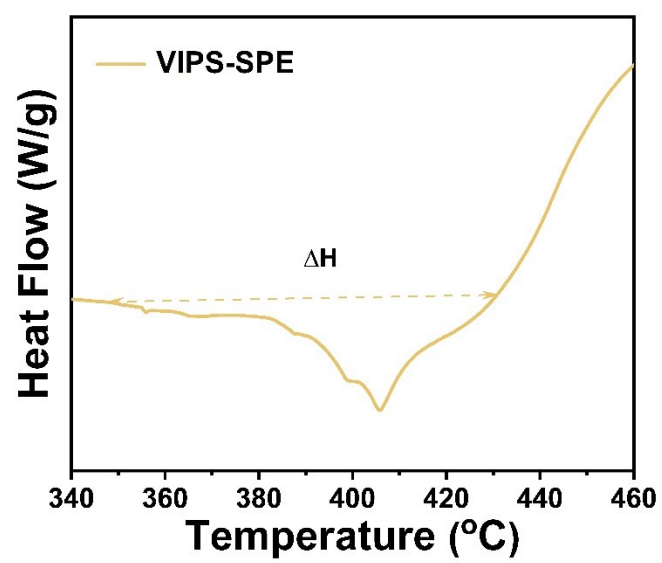
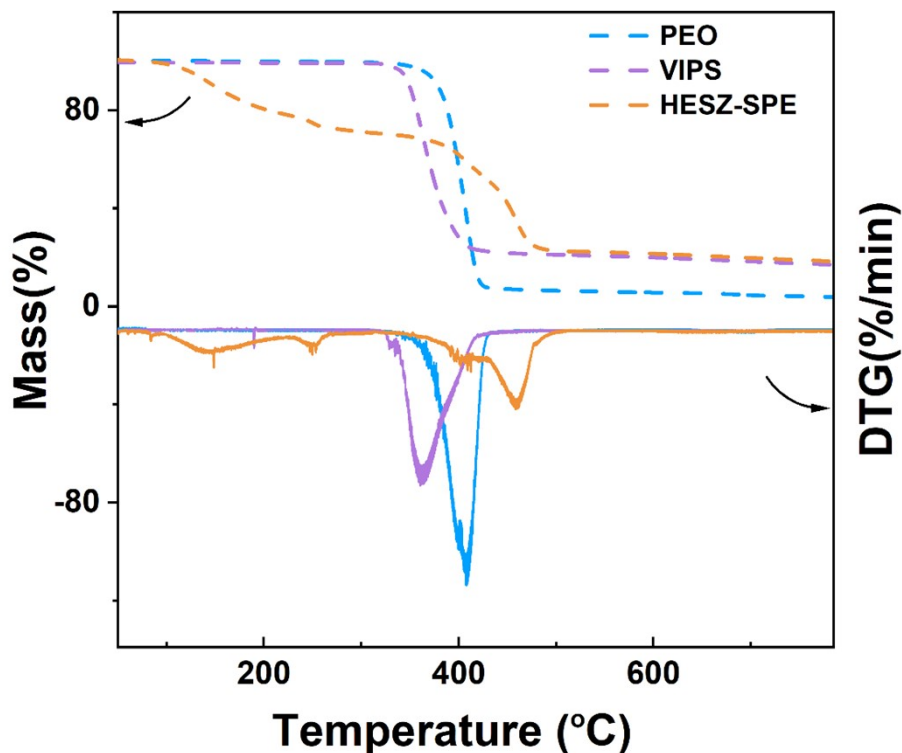


Figure S6. DSC of VIPS-SPE.



**Figure S7.** TGA and DSC of PEO, VIPS and designed HESZ-SPE.

The thermal stability of HESZ-SPE was further studied by TGA. As shown in Figure S7, the decomposition of polymer and salts in HESZ-SPE starts at ca. 350 °C, while the initial decomposition of pure PEO occurs at ca. 410 °C. This should be ascribed to reduced crystallinity of PEO matrix due to the interacting between the high concentrations of LiTFSI and PEO, which probably makes the peak of PEO overlap with that of LiTFSI in TGA curve. Nonetheless, HESZ-SPE membrane is thermally stable enough for SSLBs considering the stability up to 350 °C. Moreover, the weight loss of HESZ-SPE occurred with slower slope and more plateau compared to PEO confirming the thermal stability of HESZ-SPE, and the least weight loss could be attributed to the enhancement of interaction and amorphous phase. By the way, the minor weight loss of HESZ-SPE before 150 °C is due to the trapped moisture. The weight loss observed at 150–200 °C derives from the evaporation of residual solvent.

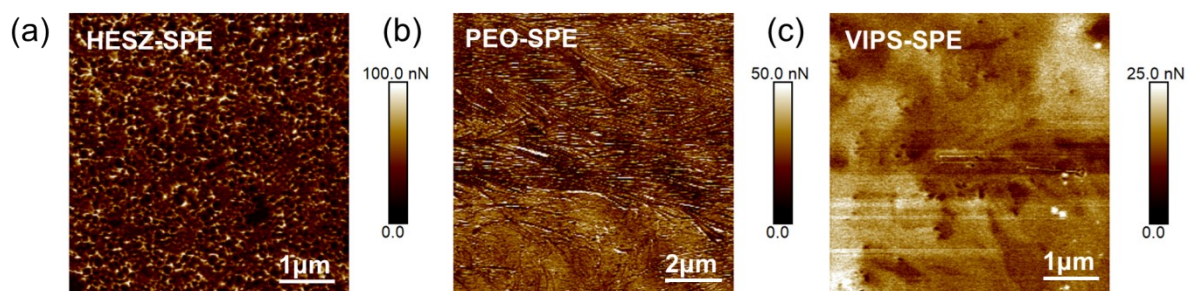
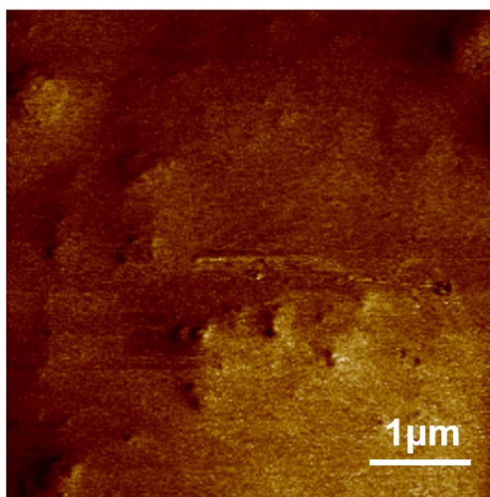
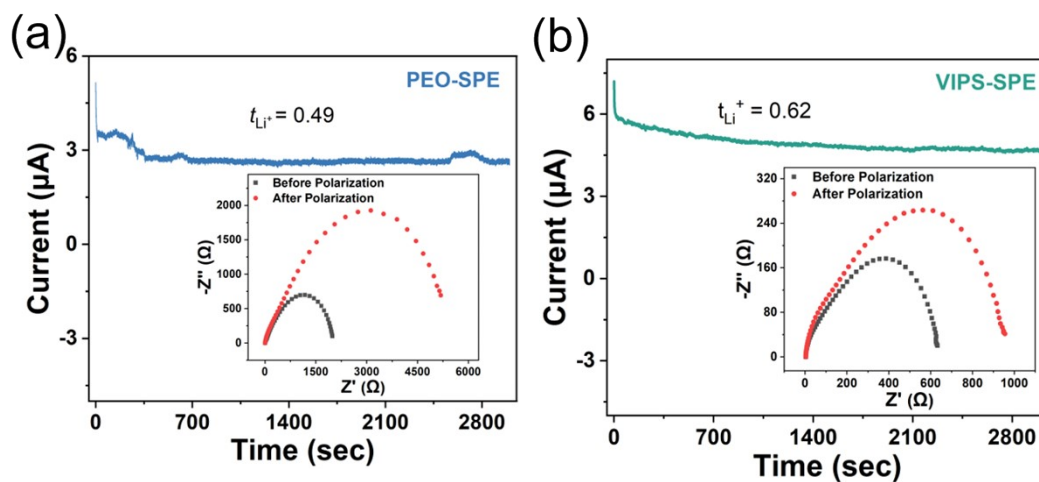


Figure S8. Adhesion force mapping by AFM of various electrolytes. (a)HESZ-SPE, (b) PEO-SPE, and (c)VIPS-SPE.



0 GPa  3 GPa

**Figure S9.** The DMT modulus of VIPS-SPE detected from AFM characterize.



**Figure S10.** Cationic transference number test results of PEO-SPE (a) and VIPS-SPE (b). Polarization (POL) result and fitted electrochemical impedance spectra (EIS) before and after POL (inset) of PEO-SPE (a) and VIPS-SPE (b).

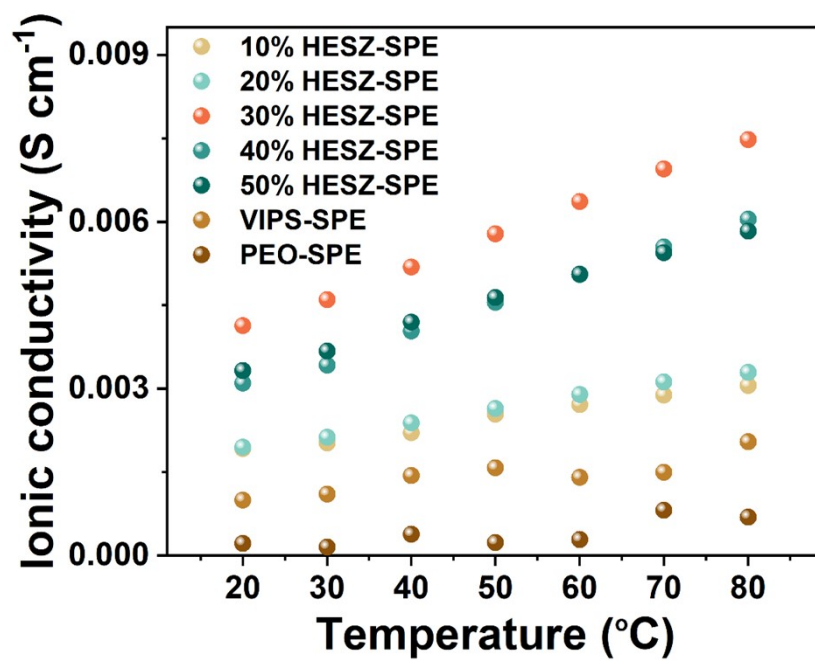


**Figure S11.** Ionic conductivities of PEO, VIPS and designed HESZ-SPE with different content of PZ at varying temperatures.

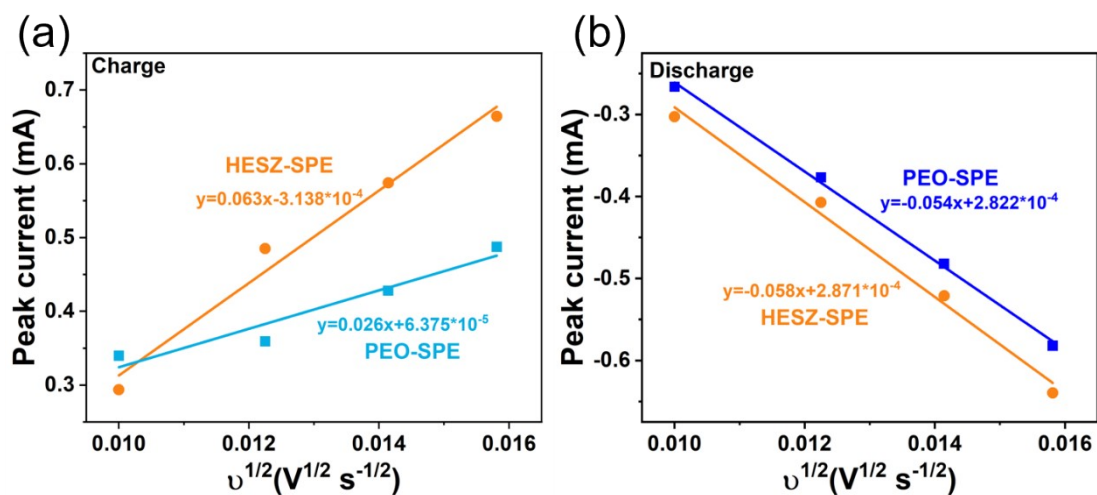


**Figure S12.** The slope curves of anodic peak currents (a) and cathodic peak currents (b) depend on the square root of scan rates for HESZ-SPE and PEO-SPE.

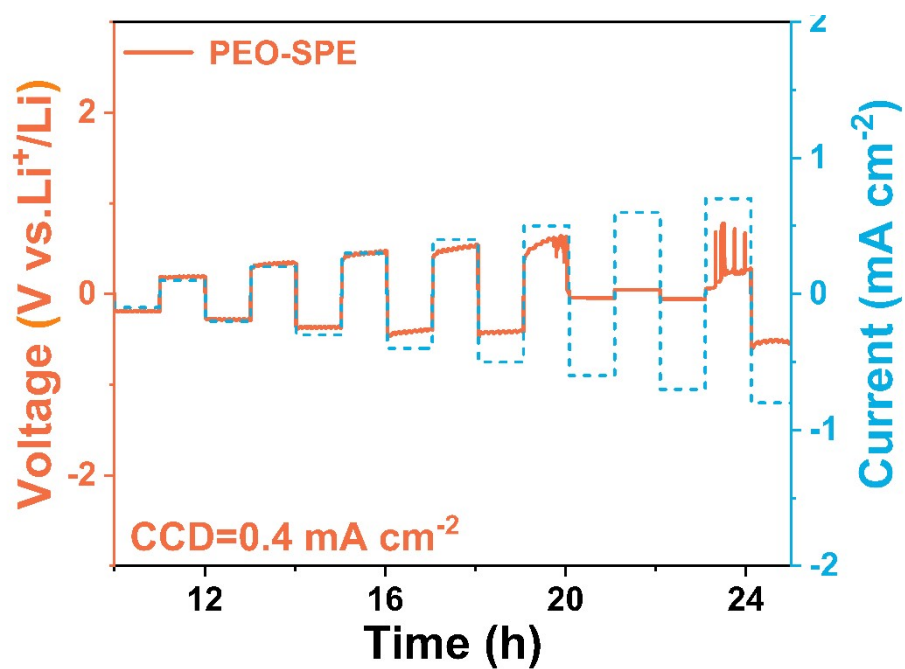


**Figure S13.** The critical current density (CCD) test of PEO-SPE at 25 °C.

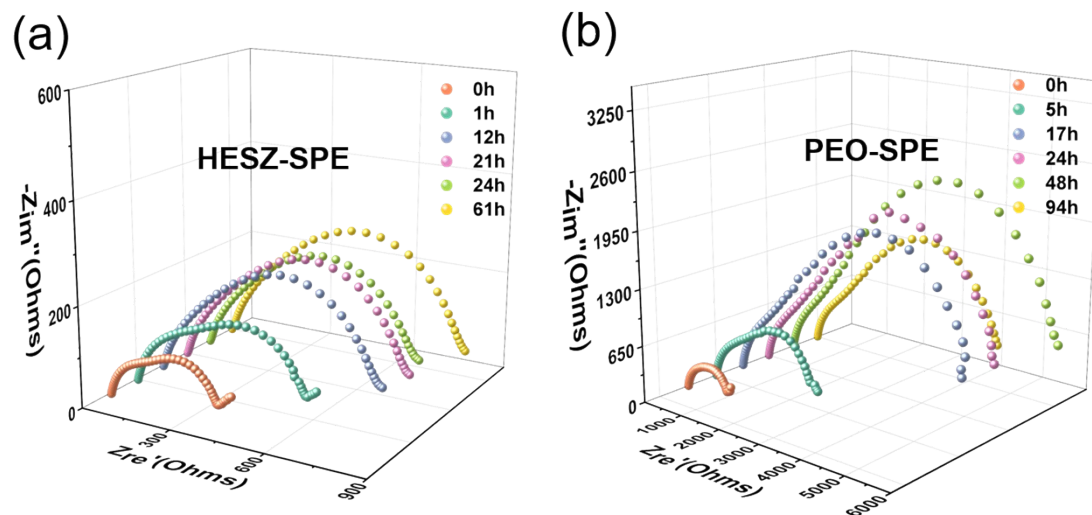


**Figure S14.** The static interfacial impedances of Li| HESZ-SPE |Li (a) and Li| PEO-SPE |Li (b) cell at different times.

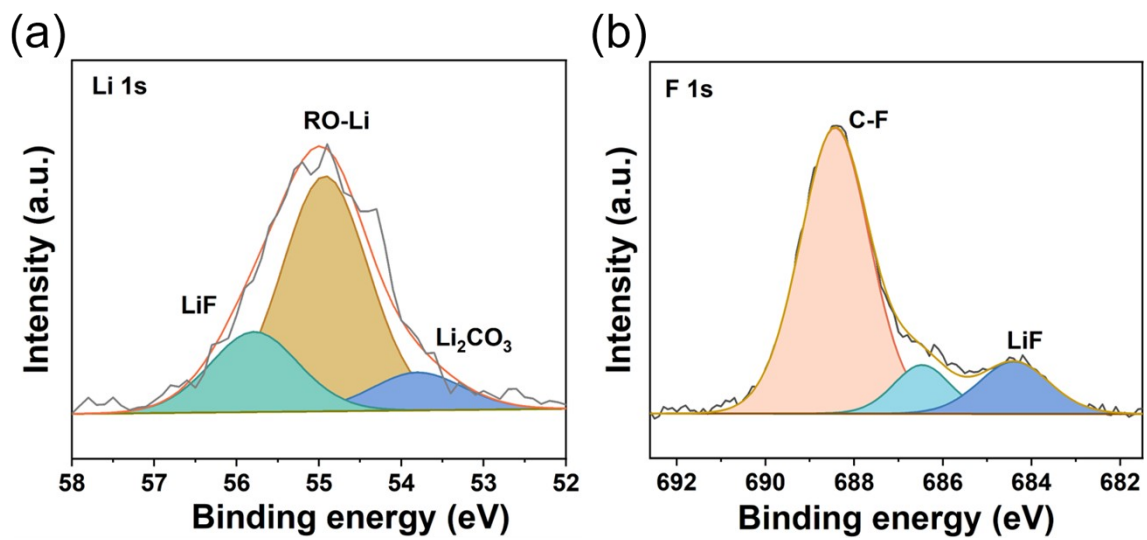
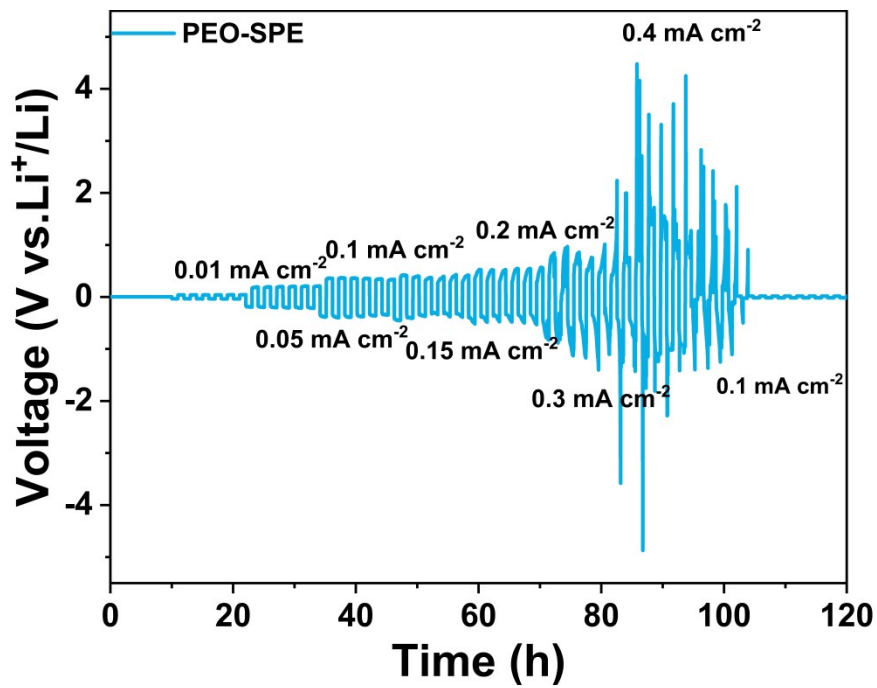
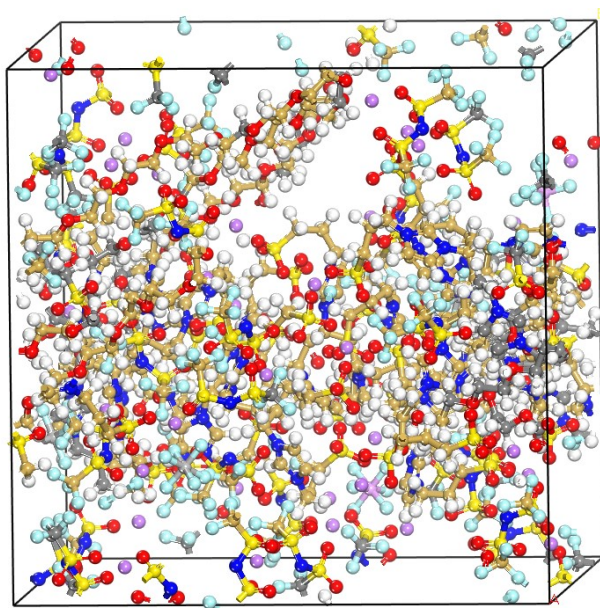


Figure S15. XPS spectra of cyclic-Li metal anodes using HESZ-SPE. (a) Li 1s, (b) F 1s.



**Figure S16.** Voltage profiles of Li/PEO-SPE/Li symmetrical batteries at varied current density.



**Figure S17.** Visualization of the origin HEMI-ASPE-Li systems ( $t = 0$  ns).

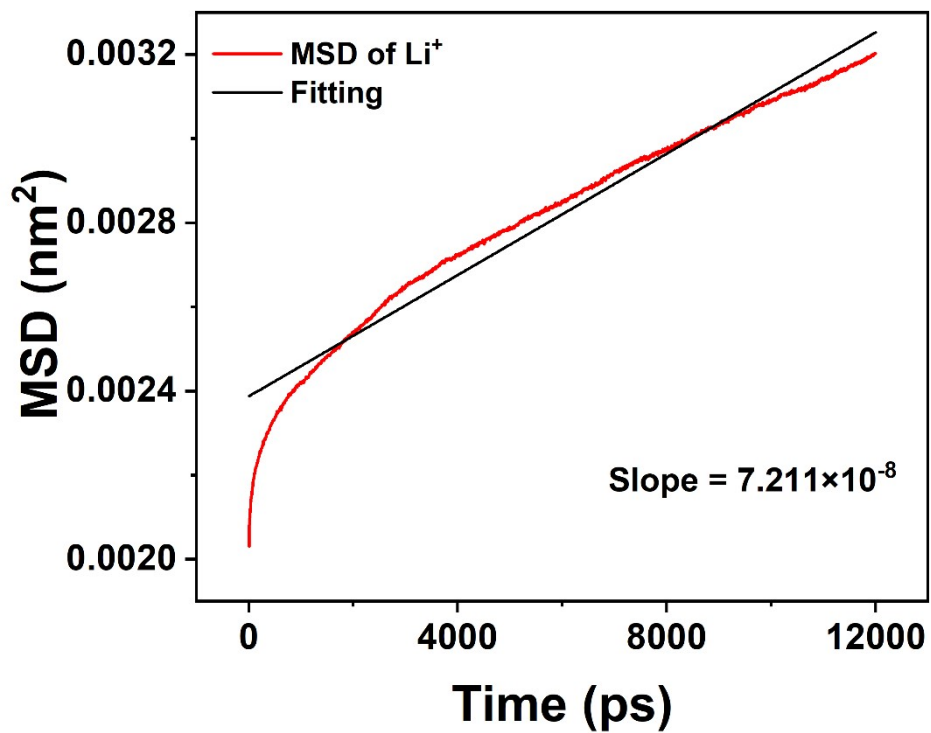


**Figure S18.** The Mean squared displacements (MSD) of Li ions in HESZ-SPE at 298 K systems.

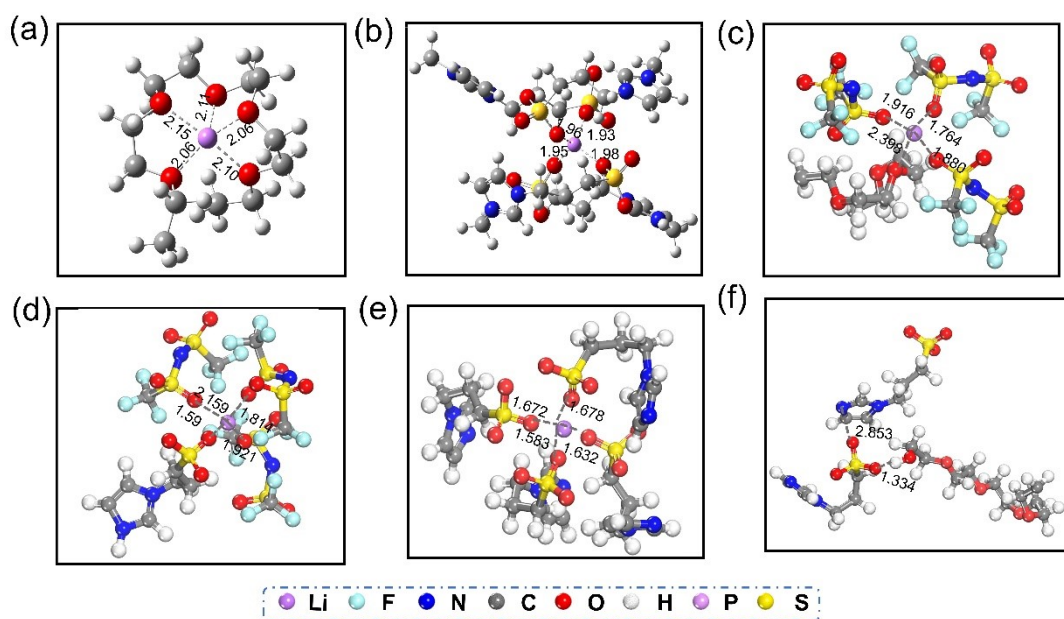


**Figure S19.** The localized zoomed-in view of the coordination structures after the simulations. (a)  $\text{Li}\cdots\text{O}$  (PEO), (b)  $\text{Li}\cdots\text{O}$  (VIPS), (c)  $\text{Li}\cdots\text{O}$  (PEO and TFSI<sup>-</sup> in HESZ-SPE), (d)  $\text{Li}\cdots\text{O}$  ( $\text{SO}_3^-$  and TFSI<sup>-</sup> in HESZ-SPE), (e)  $\text{Li}\cdots\text{O}$  ( $\text{SO}_3^-$  in HESZ-SPE), and (f)  $\text{OH}\cdots\text{O}$  (PEO,  $\text{SO}_3^-$ ).

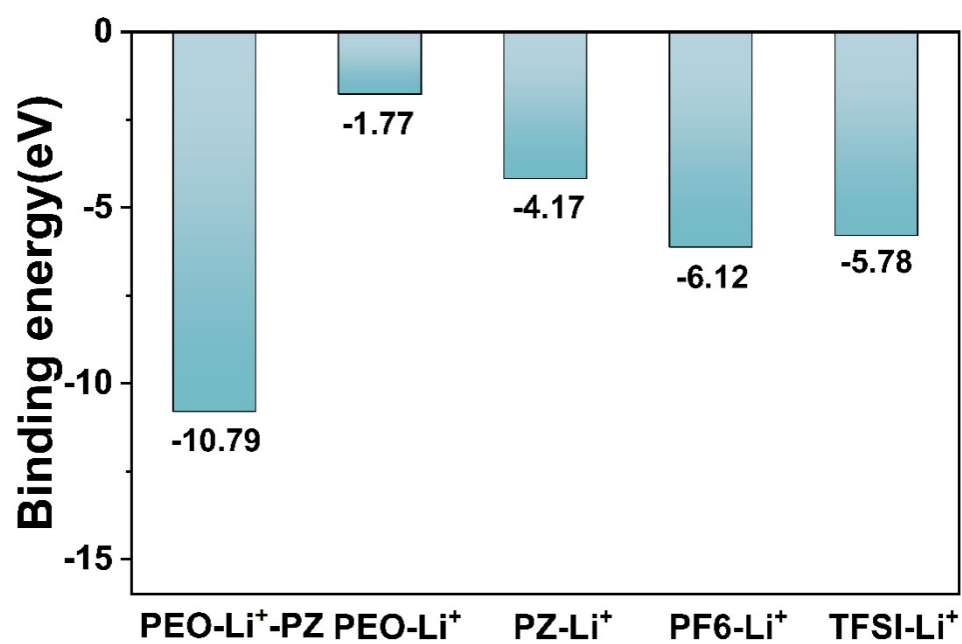


**Figure S20.** The binding energies of PEO-Li<sup>+</sup>, PZ-Li<sup>+</sup>, LiTFSI-Li<sup>+</sup> and PEO-Li<sup>+</sup>-PZ.

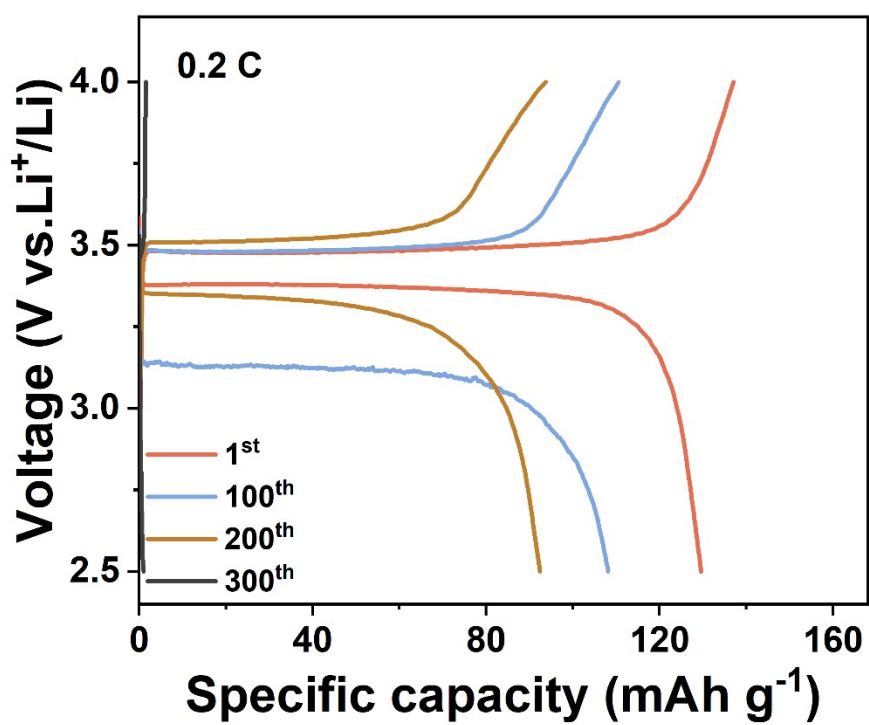


**Figure S21.** The corresponding charging and discharging curves at different cycles of full batteries with PEO-SPE at 0.2 C.

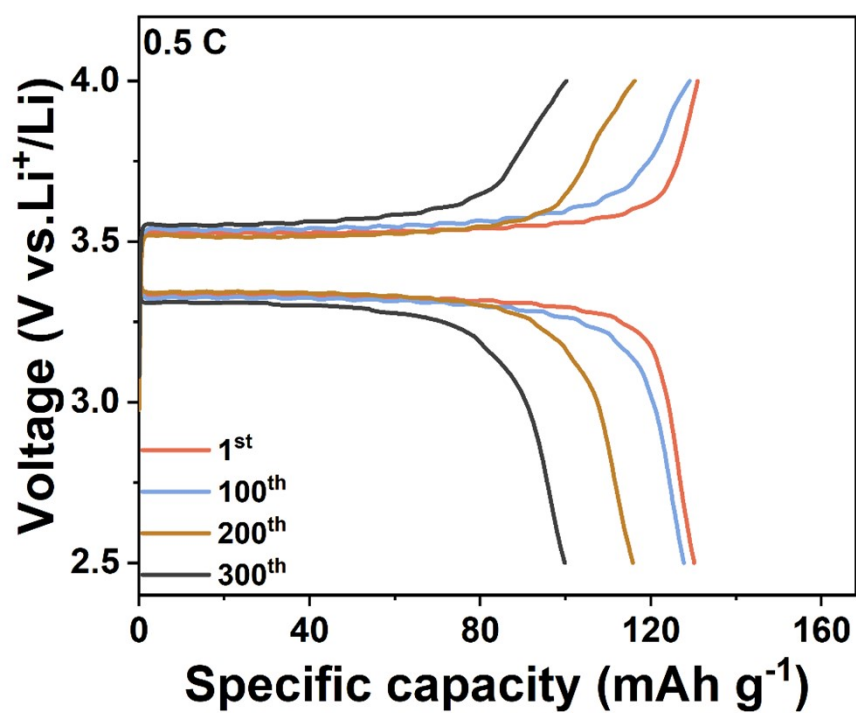


**Figure S22.** The corresponding charging and discharging curves at different cycles of full batteries with HESZ-SPZ-SPE at 0.5 C.

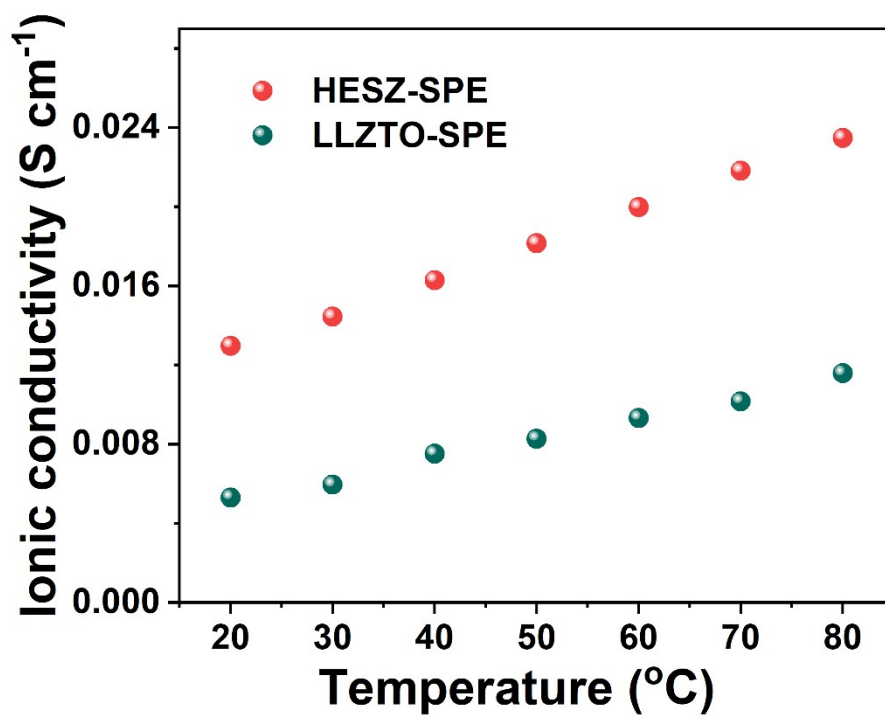


**Figure S23.** The ionic conductivity comparison results of HESZ-SPE and LLZTO-SPE.

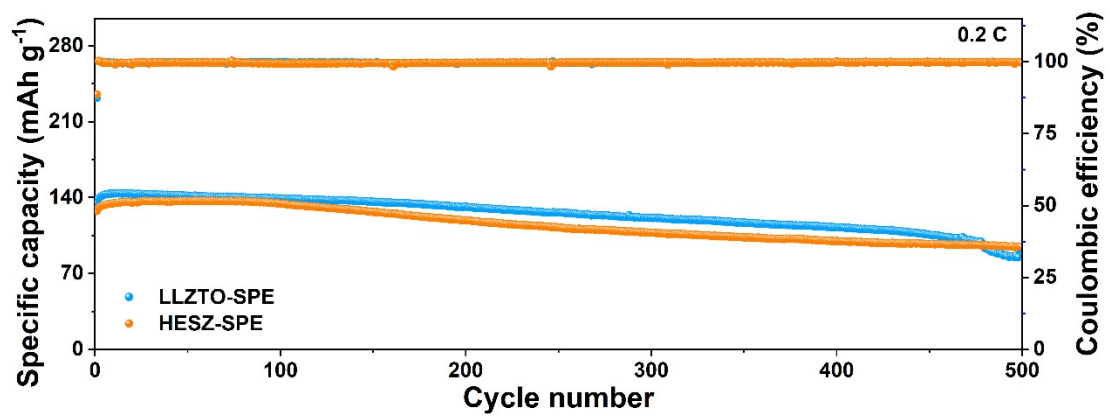


**Figure S24.** Cycling performances using HESZ-SPE and LLZTO-SPE over 500 cycles at a rate of 0.2 C and 25 °C.

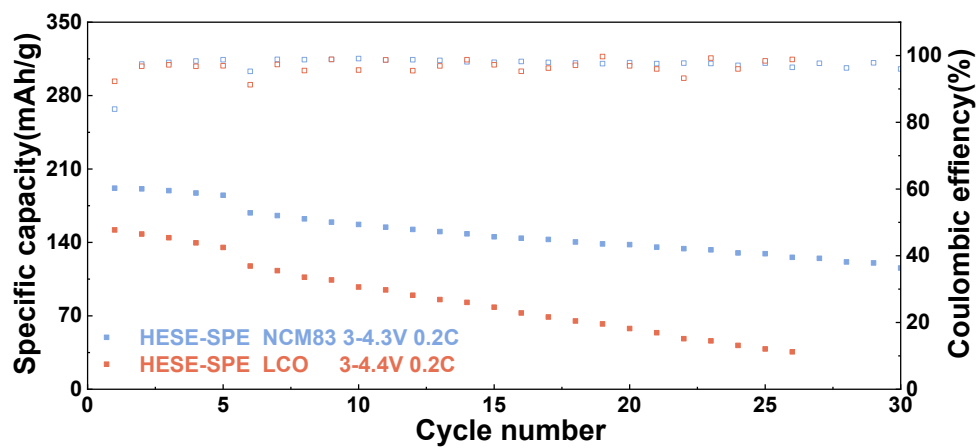


**Figure S25.** Cycling performances of Li|HESE-SPE|NCM83/LCO full batteries at 0.2 C and 25°C.

**Table S1.** The thermodynamic profiles and degree of crystallinity obtained from DSC curves of membranes

Electrolytes	$\Delta H_m/\text{J g}^{-1}$	$\chi_c/\%$
HESZ-SPE	40.88	20.14
PEO-SPE	75.72	37.30
VIPS-SPE	53.22	26.22

The crystallinity  $\chi_c$  of polymer composite electrolyte is calculated by Equation (14).<sup>[9]</sup>

$$\chi_c = \frac{\Delta H_m}{\Delta H_{peo}} \times 100\% \quad (14)$$

Where  $\chi_c$  represents the relative percentage of crystallinity of PEO-based polymer electrolyte,  $\Delta H_m$  represents the melting enthalpy of electrolyte that can be obtained through the melting temperature ( $T_m$ ) peak area of DSC curves, and  $\Delta H_{PEO}$  is the melting enthalpy of PEO matrix with 100% crystallization, which is 203 J/g.

**Table S2.** Super-high ionic conductivity and advanced Li<sup>+</sup> transference number of SSLMBs using HESZ-SPE could also be confirmed compared with other different reported results.

<b>Strategies</b>	<b>Transference number</b>	<b>Ion conductivity (S·cm<sup>-1</sup>)</b>	<b>Temperature (°C)</b>	<b>Ref.</b>
HEMI-ASPE-Li	0.63	4.56E-4	70	[3]
C4P-PEO-LiTFSI	0.70	1.9E-3	60	[4]
AMIC	0.67	1.78E-4	60	[5]
PEO-LiTFSI-CsPbI <sub>3</sub>	0.57	1.4E-4	30	[6]
PEO-TOC	0.51	5.5E-5	30	[7]
A-ISPE	0.67	7.77E-4	25	[8]
EFA-G	0.33	9.87E-4	30	[9]
PLNH-SPE	0.41	7.4E-4	30	[10]
PTMG-HDI-BHDS/LiFSI	0.81	2.4E-4	30	[11]
HESZ-SPE-Li	0.86	4.599E-3	30	this work

**Table S3.** Simulation parameters of HESZ-SPE-Li and PEO-SPE-Li for AS-LMBs.

<b>Parameters</b>	<b>HESZ-SPE-Li</b>	<b>PEO-SPE-Li</b>	<b>Unit</b>
Ionic conductivity ( $\sigma$ )	4.599E-3	7.427E-5	S·cm <sup>-1</sup>
Salt concentration ( $c$ )	1472.3	1472.3	mol·m <sup>-3</sup>
Transference number ( $t_{\text{Li}^+}$ )	0.86	0.49	-
Cation diffusion coefficient ( $D^+$ )	7.106E-12	1.226E-12	m <sup>2</sup> ·s <sup>-1</sup>
Anion diffusion coefficient ( $D^-$ )	6.076E-12	1.226E-12	m <sup>2</sup> ·s <sup>-1</sup>

**Table S4.** Simulation conditions of HESZ-SPE-Li and PEO-SPE-Li for SSLMBs.

<b>Parameters</b>	<b>HESZ-SPE-Li</b>	<b>PEO-SPE-Li</b>	<b>Unit</b>
Diameter of solid electrolyte ( $d$ )	50	50	$\mu\text{m}$
The thickness of solid electrolyte ( $H$ )	200	200	$\mu\text{m}$
Operating temperature ( $T$ )	30	30	$^{\circ}\text{C}$

## References

- [1] Y. Su, X. Rong, H. Li, X. Huang, L. Chen, B. Liu and Y. S. Hu, *Advanced Materials*, 2022, **35**.
- [2] Y. Su, X. Rong, A. Gao, Y. Liu, J. Li, M. Mao, X. Qi, G. Chai, Q. Zhang, L. Suo, L. Gu, H. Li, X. Huang, L. Chen, B. Liu and Y.-S. Hu, *Nature Communications*, 2022, **13**.
- [3] J. Wan, J. Xie, X. Kong, Z. Liu, K. Liu, F. Shi, A. Pei, H. Chen, W. Chen, J. Chen, X. Zhang, L. Zong, J. Wang, L.-Q. Chen, J. Qin and Y. Cui, *Nature Nanotechnology*, 2019, **14**, 705-711.
- [4] Y. Su, F. Xu, X. Zhang, Y. Qiu and H. Wang, *Nano-Micro Letters*, 2023, **15**.
- [5] T. Lu, F. Chen, *Journal of Computational Chemistry* 2011, **33**, 580-592.
- [6] X. Zhang, Q. Su, G. Du, B. Xu, S. Wang, Z. Chen, L. Wang, W. Huang and H. Pang, *Angewandte Chemie International Edition*, 2023, **62**.
- [7] J. Han, M. J. Lee, J. H. Min, K. H. Kim, K. Lee, S. H. Kwon, J. Park, K. Ryu, H. Seong, H. Kang, E. Lee, S. W. Lee and B. J. Kim, *Advanced Functional Materials*, 2024, **34**.
- [8] Z. Jiang, C. Li, T. Yang, Y. Deng, J. Zou, Q. Zhang and Y. Li, *ACS Energy Letters*, 2024, **9**, 1389-1396.
- [9] T. Wang, B. Chen, C. Liu, T. Li and X. Liu, *Angewandte Chemie International Edition*, 2024, **63**.